

Supplementary Information

π - π Conjugation Promoted Nanocatalysis for Cancer Therapy Based on Covalent Organic Framework

*Shuncheng Yao,^{ab} Xingru Zhao,^{ab} Xingyi Wan,^{ab} Xueyu Wang,^a Tian Huang,^a Jiaming Zhang,^{ab} Linlin Li^{*ab}*

^a Beijing Institute of Nanoenergy and Nanosystems, Chinese Academy of Sciences, Beijing 101400, P. R. China.

^b School of Nanoscience and Technology, University of Chinese Academy of Sciences, Beijing 100049, P. R. China.

*Corresponding author: Prof. Linlin Li

E-mail: lilinlin@binn.cas.cn

METHODS

Materials

5,10,15,20-Tetrakis(4-aminophenyl)-21H,23H-porphine (TAPP), ferrous chloride (FeCl_2), 2,5-Dihydroxy-terephthalaldehyde (DHPA), multi-walled CNTs, and carboxylic multi-walled carbon nanotubes (Carboxyl CNTs) were acquired from Aladdin reagent (Shanghai) Co., Ltd. Acetonitrile, 1-ethyl-3-(3-dimethylaminopropyl) carbodiimide (EDC), N-hydroxysulfosuccinimide (NHS), mesitylene, anhydrous ethanol, acetic acid, 1,4-dioxane, tetrahydrofuran, and acetone were purchased from Shanghai McLin Biochemical Technology Co., Ltd. 3,3',5,5'-Tetramethylbenzidine (TMB), dimethyl sulfoxide (DMSO), 3-diphenylisobenzofuran (DPBF) were acquired from Sigma-Aldrich Inc. (St. Louis, MO). Calcein AM/PI Cell Viability/Cytotoxicity Assay Kit, 2',7'-Dichlorofluorescein diacetate, mouse monoclonal IgG1, 4',6-diamidino-2-phenylindole (DAPI), and 3-(4,5-Dimethyl-2-Thiazolyl)-2,5-diphenyl tetrazolium bromide (MTT) was purchased from Beijing Solab Technology Co., Ltd. APC anti-mouse CD4, PE anti-mouse CD80, APC anti-mouse CD86, FITC anti-mouse CD11c, FITC anti-mouse CD3, PE anti-mouse CD8a, mouse IL-6 Elisa kit, and mouse TNF- α ELISA kit were purchased from

Beijing Dakewei Biotechnology Co., Ltd. Sheep blood were acquired from Beijing Land Bridge Technology Co., Ltd.

Preparation of TAPP-Fe

TAPP (134.8 mg) was dissolved in acetonitrile (100 mL) to form a clear purple-red solution in 250 mL round bottom flask and FeCl₂ (25 mg) was subsequently added. The above solution was refluxed for 24 h under nitrogen protection. The residual solution was cooled to 0 °C, and then the purple black precipitation was collected. Finally, the TAPP-Fe was dried at 60 °C for further use.

Preparation of TAPP-Fe-CNT

Carboxyl CNTs (0.1 g) was dispersed in deionized water (10 mL), and then 70 mg EDC and 30 mg NHS were added and mixed under magnetic stirring at 25 °C for 1 h. Deionized water (10 mL) containing TAPP-Fe was added to the above solution and the mixture was heated at 60 °C for 24 h, washed with deionized water, and dried to obtain the TAPP-Fe-CNT.

Preparation of COF-CNT

A glass tube was filled with TAPP-Fe (13.5 mg), MWCNTs (6.25 mg), 0.5 mL of mesitylene, and 2,5-Dihydroxy-terephthalaldehyde (HTPAL, 5.6 mg) dispersed in anhydrous ethanol (0.5 mL). Aqueous acetic acid (3 M; 0.1 mL) was then added into the suspension. The tube was carefully degassed by three freeze–pump–thaw cycles and then sealed under vacuum. The reaction mixture was sonicated for 60 min. After being thermostated at 70 °C in an oil bath and stirred for 24 h, black solid precipitates were obtained. After centrifugation, repeated washing with 1,4-dioxane, tetrahydrofuran and acetone, and drying at 60 °C under vacuum for 12 h, the final product of COF-CNT was collected.

DFT simulation

All the calculations were performed in the framework of the density functional theory with the projector augmented plane-wave method, as implemented in the Vienna ab initio simulation package¹. The generalized gradient approximation proposed by Perdew, Burke, and Ernzerhof was selected for the exchange-correlation potential². The cut-off energy for plane wave was set to 400 eV. The energy criterion was set to 10⁻⁵ eV in iterative solution of the Kohn-Sham equation. A super large cubic box with the

lattice length of 45 Å was built to avoid artificial interaction between periodic images. The Brillouin zone integration was performed using a 1×1×1 k-mesh. The spin polarization was considered. All the structures were relaxed until the residual forces on the atoms had declined to less than 0.02 eV/Å. The free energies of the intermediates at 298.15 K were obtained using $\Delta G = \Delta E + \Delta ZPE - T\Delta S$ according to previous work³, where ΔE is the binding energy of adsorption species, ΔZPE and ΔS are the zero point energy changes and entropy changes. Electrostatic potentials were computed for isolated molecules in vacuum unless noted otherwise. Molecule “surfaces” were taken to be the 0.001 e/bohr³ density isosurface. This isosurface encompassed approximately 96% of the electronic charge, which is considered as the standard for calculating the electrostatic potential.

Electrochemical measurements

Cyclic voltammograms (CV) and electrochemical impedance spectroscopy (EIS) of TAPP-Fe-CNT and COF-CNT were conducted with a CHI 660E electrochemical workstation (Chenhua Instrument, Shanghai, China) in a standard three-electrode system with a glassy carbon electrode as the working electrode, Pt plate as the counter electrode, and a saturated calomel electrode (SCE) as a reference electrode. The electrolyte was a pH 6.5 PBS solution. A 100 μL COF-CNT suspension (1 mg mL⁻¹) was dropped on the surface of the glassy carbon electrode and dried at room temperature for CV measurements. EIS was performed with a 100 μL COF-CNT suspension (1 mg mL⁻¹) dropped on the surface of the glassy carbon electrode and dried at room temperature within the frequency range from 10⁻¹ to 10⁴ Hz with a bias potential of -1.5 V.

Calculation of kinetics constants (K_m) and catalytic constant (K_{cat})

The kinetics constants K_m was calculated by fitting the reaction velocity values and the substrate concentrations to the Michaelis–Menten equation as follows:

$$v = \frac{(v_{max} \times [S])}{(K_m + [S])}$$

where v is the initial reaction velocity and V_{max} is the maximal reaction rate that is observed at the saturating substrate concentrations. $[S]$ is the concentration of the substrate and K_m is the Michaelis

constant. K_m reflects the affinity of the catalyst to its substrate and is defined as the substrate concentration at half the maximum rate.

The catalytic constant (K_{cat}) is calculated using the following equation:

$$K_{cat} = v_{max}/[E]$$

where K_{cat} is the rate constant defining the maximum number of substrate molecules converted to product per unit of time. $[E]$ is the catalyst concentration.

Photothermal conversion performance and photothermal conversion efficiency (η)

For measuring the photothermal conversion performance of the COF-CNT, 1 mL aqueous dispersion of nanomaterials ($60 \mu\text{g mL}^{-1}$) in a glass bottle was irradiated with an 808 nm NIR laser at a power density of 1 W cm^{-2} for 10 min. A thermocouple probe was inserted into the aqueous solution perpendicular to the path of the laser for real-time temperature recording. The photothermal properties of COF-CNT with different concentrations and irradiation powers, and the thermal cycle performance of COF-CNT was determined under the same way.

The photothermal conversion efficiency (η) of COF-CNT was determined. Detailed calculation is given as following:

Based on the total energy balance of this system:

$$\sum_i m_i C_{p,i} \frac{dT}{dt} = Q_{COF-CNT} + Q_s - Q_{loss} \quad (1)$$

where m and C_p are the mass and heat capacity of solvent (water), respectively. T is the solution temperature. $Q_{COF-CNT}$ is the photothermal energy input by COF-CNT:

$$Q_{COF-CNT} = I(1 - 10^{-A_\lambda})\eta \quad (2)$$

where I is the laser power, A_λ is the absorbance of COF-CNT at the wavelength of 808 nm, and η is the conversion efficiency from the absorbed light energy to thermal energy.

Q_{loss} is thermal energy lost to the surroundings:

$$Q_{loss} = hA\Delta T \quad (3)$$

where h is the heat transfer coefficient, A is the surface area of the container, and ΔT is the temperature change, which is defined as $T - T_s$ (T and T_s are the solution temperature and ambient temperature of the surroundings, respectively).

$$Q_{COF-CNT} + Q_s = Q_{loss} = hA\Delta T_{max} \quad (4)$$

where ΔT_{max} is the temperature change at the maximum steady-state temperature. According to the Eq. 2 and Eq. 4, the photothermal conversion efficiency (η) can be determined:

$$\eta = \frac{hA\Delta T_{max} - Q_s}{I(1 - 10^{-A\lambda})} \quad (5)$$

$\theta = \frac{\Delta T}{\Delta T_{max}}$. Then put the calculated θ into Eq. 1 and rearrange Eq. 1:

$$dt = - \sum_i m_i C_{p,i} \frac{1}{hA} \frac{d\theta}{\theta} \quad (6)$$

When the laser was shut off, $Q_{COF-CNT} + Q_s = 0$. Then integrating Eq. 6 to give the expression:

$$t = - \sum_i m_i C_{p,i} \frac{\ln \theta}{hA} \quad (7)$$

Thus, hA can be determined by applying the linear time data from the cooling period vs $-\ln \theta$. Substituting hA value into Eq. 5, the photothermal conversion efficiency (η) of COF-CNT can be calculated.

Detection of 1O_2 for PDT performance

The generation of 1O_2 under NIR light irradiation was detected using 3-diphenylisobenzofuran (DPBF) as the probe, whose fluorescence would be diminished in the presence of 1O_2 . 20 μ L of DPBF (2 mg mL⁻¹) in DMSO was added into 1 mL of COF-CNT (25 μ g mL⁻¹). The mixed solution was then irradiated with a 808 nm laser (1 W cm⁻²), during which the fluorescence spectrum of the mixture was measured at different time intervals. The 1O_2 generation ability was calculated as A_1/A_0 , where A_0 and A_1 are the absorption intensity of the mixed solutions at 415 nm before and after laser irradiation, respectively.

Dissolved O₂ (DO) detection

For detecting the O₂ production of COF-CNT (CAT-like activity), H₂O₂ (100 μ M) was added into COF-CNT (60 μ g mL⁻¹) aqueous suspension. Then, the concentration of dissolved O₂ was monitored by a

portable dissolved oxygen meter (Leici JPSJ-606L). O₂ production at different H₂O₂ concentrations (12.5 μM, 25 μM, 50 μM, and 100 μM) was also measured.

·OH detection

Typically, 10 mg of TMB was dissolved in 1 mL of DMSO. Aqueous suspension of nanomaterials (1 mg mL⁻¹; 50 μL) and 30% H₂O₂ (10 μL) were mixed and added to PBS (1 mL; pH=6.5). The samples were taken for UV-vis absorption spectrum measurements at 1 min intervals. In order to study the effect of temperature and pH on the catalytic performance, the detection was carried out under different temperatures (20, 30, 40, 50 and 60 °C) and pH values (4, 5, 6, 6.5, and 7), respectively.

Cell culture

Murine 4T1 breast cancer cells and mouse embryonic fibroblasts (3T3) were obtained from the Peking Union Medical College Hospital (Peking, China). 4T1 cells were maintained in high-glucose DMEM (Gibco) supplemented with 10% fetal bovine serum (FBS) (Gibco) and 1% penicillin/streptomycin at 37 °C with 5% CO₂. 3T3 cells were cultured in high-glucose DMEM supplemented with 10% FBS, 1% L-glutamine and 1% penicillin/streptomycin at 37 °C with 5% CO₂.

Co-staining with Calcein-AM and PI

The 4T1 cells on CLSM-exclusive culture disk (35 mm) were incubated with COF-CNT (60 μg mL⁻¹) for 6 h, washed with PBS twice before Calcein-AM and PI were added. After incubation with Calcein-AM and PI for 30 min, the cells were washed with PBS twice. The cells in the COF-CNT+H₂O₂ group were incubated with H₂O₂ (100 μM) for 3 min. And the cells in the COF-CNT+NIR and COF-CNT+NIR+H₂O₂ group were exposed to 808 nm laser irradiation (1.0 W cm⁻²) for 3 min. The green and red fluorescence were observed on a Confocal laser scanning microscope (Leica SP8).

Intracellular ROS level

4T1 cells were seeded in CLSM-exclusive culture disk (35 mm). After different treatments, the intracellular ROS level was determined by detecting the fluorescence of 2,7-dichloro-fluorescein (DCF) that was generated by the oxidation of DCFH-DA. Then the green DCF fluorescence signal was captured by CLSM.

Co-staining with calreticulin (CRT) and nuclei

4T1 cells were seeded in CLSM-exclusive culture disk (35 mm) and incubated for 24 h. After different treatments, the cells were fixed with 4% formaldehyde for 20 min, washed with PBS twice, and sealed with goat serum (1%) for 1 h. The cells were incubated with 500 μ L mouse monoclonal IgG1 (2 μ M) for 12 h, and washed with PBS twice. Next, the cells were incubated with 500 μ L 1: 1000 diluted Goat Anti-Mouse IgG (H+L) for 2 h. Then DAPI (100 ng/mL) was used to stain the nuclei for 30 min. Finally, the cells were washed with PBS twice and observed by CLSM.

Cell viability

MTT assay was used to detect cell viability. 4T1 cells were seeded at a density of 1×10^5 cells per well in 96-well plates. After 24 h, the cells were suffered from different treatments. After the treatments, 20 μ L of MTT solution (5 mg mL⁻¹) in PBS (pH 7.4) was added to each well and the cells were incubated for another 2 h. Then, the supernatant was removed carefully, followed by adding 150 μ L of DMSO to each well to dissolve the MTT-formazan crystals. Next, light absorbance (abs.) at $\lambda=490$ nm was recorded on an enzyme-labeled instrument (imark, BIO-RAD). The average value of four independent experiments was calculated and the relative cell viability was calculated by the following equation: cell viability (%)=(abs. value of treatment group/ abs. value of control) \times 100.

In vitro hemolysis

Different concentrations of COF-CNT suspension (1, 2, 3, 4, and 5 mg mL⁻¹) was added into fresh sheep blood (1 mL), incubated for 2 hours at 37 °C, and then centrifuged for 10 min (3000 rpm). PBS and sheep blood (1 mL) containing 50 μ m ACK split red solution were used as the negative control and the positive control, respectively. The absorption values were determined at 570 nm. The percentage of hemolysis was calculated following: hemolysis%=(sample absorbance–negative control absorbance)/(positive control absorbance–negative control absorbance) \times 100.

Animals

BALB/c female mice aged ~6 weeks were provided by Beijing Charles River Laboratories, and the procedures for handling the animals firmly stick to the “Beijing Administration Rule of Laboratory

Animals” and the national standards “Laboratory Animal Requirements of Environment and Housing Facilities (GB 14925-2001)”

In vivo systematic toxicity

For the evaluation of in vivo systematic toxicity, mice were intravenously injected with COF-CNT under different concentrations. Two weeks later, the mice were euthanized and their main organs including heart, liver, spleen, lung, and kidney were collected and fixed with 10% formalin. After being embedded in paraffin, the tissue samples were sliced (8 μm) before further histological analysis by standard hematoxylin and eosin (H&E) staining procedure.

Tumor therapy in vivo

The in vivo anticancer effect on BALB/c mice with subcutaneous 4T1 tumors were investigated. The mice were subcutaneously injected with 4T1 cells (5×10^5 ; suspended in 100 μL PBS) at the subcutaneous area of the left lower abdomen. When the tumors were reached ~ 100 -200 mm^3 in volume, the mice were randomly divided into four groups, and each group involved seven mice. They were treated as follows: 1) control group: intratumoral injection of PBS (100 μL); 2) NIR group: local injection of PBS (100 μL) and then irradiated with NIR light (808 nm; 1.0 W cm^{-2} ; 5 min); 3) COF-CNT group: local injection of COF-CNT (100 μL ; 1mg mL^{-1}); 4) COF-CNT+NIR group: local injection of COF-CNT (100 μL ; 1mg mL^{-1}) and then irradiated with NIR light (808 nm; 1.0 W cm^{-2} ; 5 min). Each mouse was earmarked and followed individually throughout the whole experiment. The tumor volume and body weight were recorded until the euthanasia. After 14 days of treatment, the mice were sacrificed and the major organs and tumors were collected for further pathological analysis by H&E staining and Ki67 immunohistochemistry (for tumor tissues only).

Flow cytometry analysis

To detect the immune cells in tumors, tumors were harvested from the treated mice. Then single-cell suspension was prepared by tissue homogenate with digestive enzyme (Liberase TL Research Grade 10). After that, the cells were washed with PBS (pH 7.4) and filtrated with cell sieve of 200 mesh. The remained cells were washed twice, diluted at $10^6/100 \mu\text{L}$ and stained with APC anti-CD4, FITC anti-CD3,

PE anti-CD8a, FITC anti-CD11c, PE anti-CD80, and APC anti-CD86, respectively, according to the manufacturer's protocols. Finally, flow cytometry analysis was performed according to the manufacturer's instruction (BD LSRFortessa).

Immunohistochemistry

Heart, liver, spleen, lung, kidney and tumors were fixed in 10% formalin and the fixed tissues were embedded in paraffin, from which continuous 8 μ m sections were prepared. H&E staining was carried out based on the standard protocol. For immunohistochemistry, a Ki-67 monoclonal antibody was used. The images were acquired with an optical microscope.

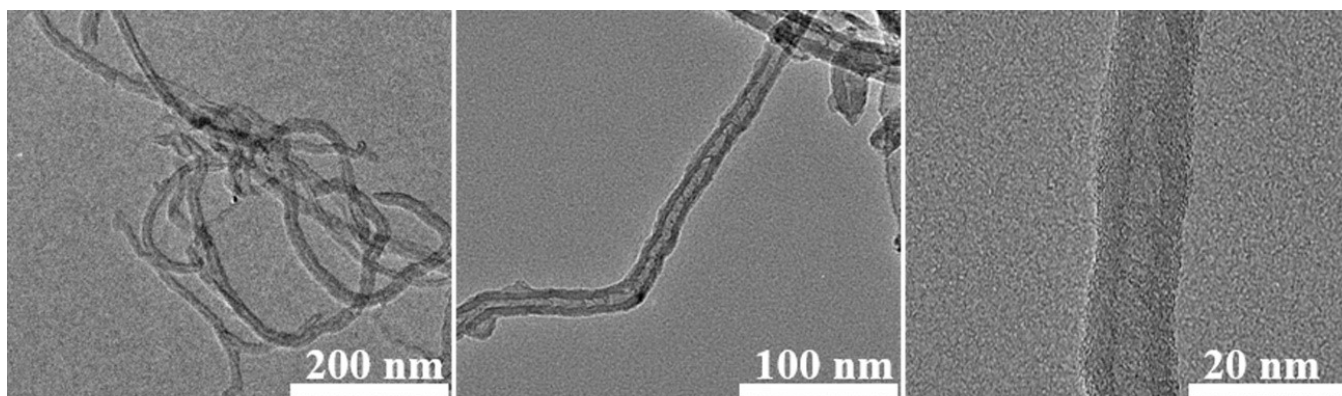
Cytokine detection

Serum samples were isolated from mice after different treatments and diluted for analysis. Tumor necrosis factor (TNF- α , BioLegend) and IL-6 (BioLegend) were analyzed with ELISA kits according to vendors' protocols.

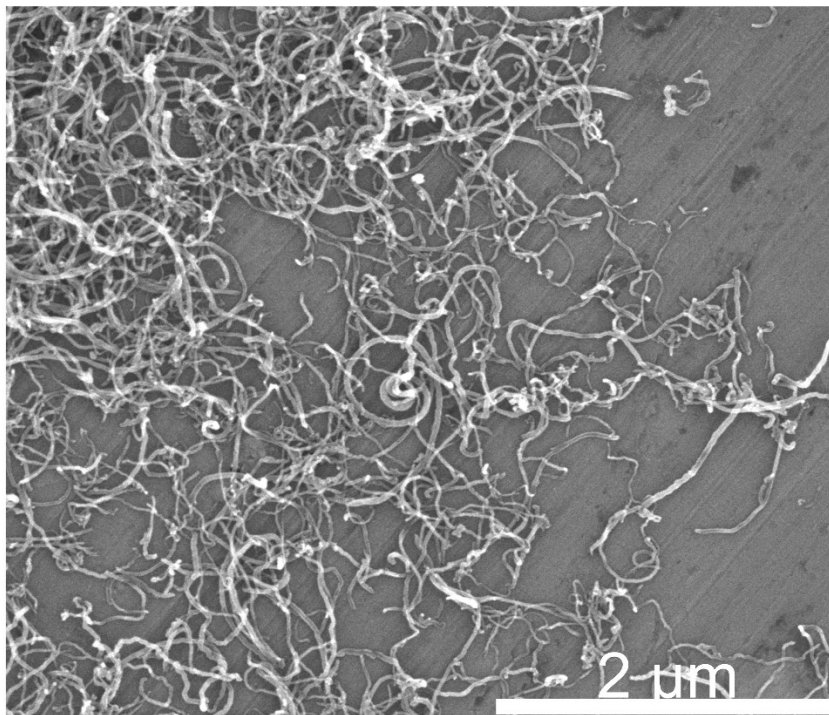
Statistical analysis

All data were expressed as mean \pm s.d. error of the mean. The statistical difference between different groups of data was evaluated by one-way ANOVA, and $p < 0.05$ was considered to be statistically significant. Asterisk (*) denotes statistical significance between bars (* $p < 0.05$, ** $p < 0.01$, *** $p < 0.001$) conducted using GraphPad Prism 6.0.

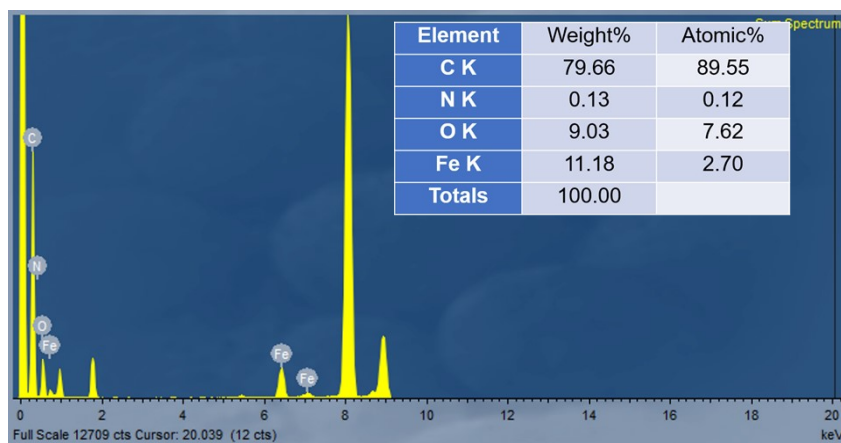
Supplementary Figures



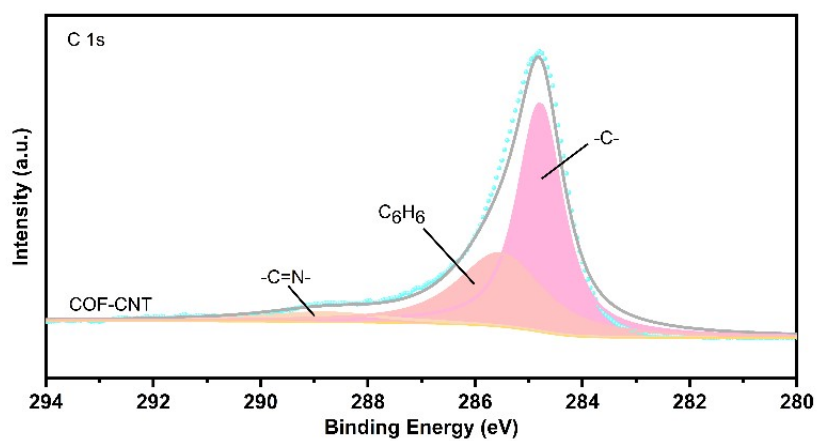
Supplementary Fig. 1. TEM images of TAPP-Fe-CNT.



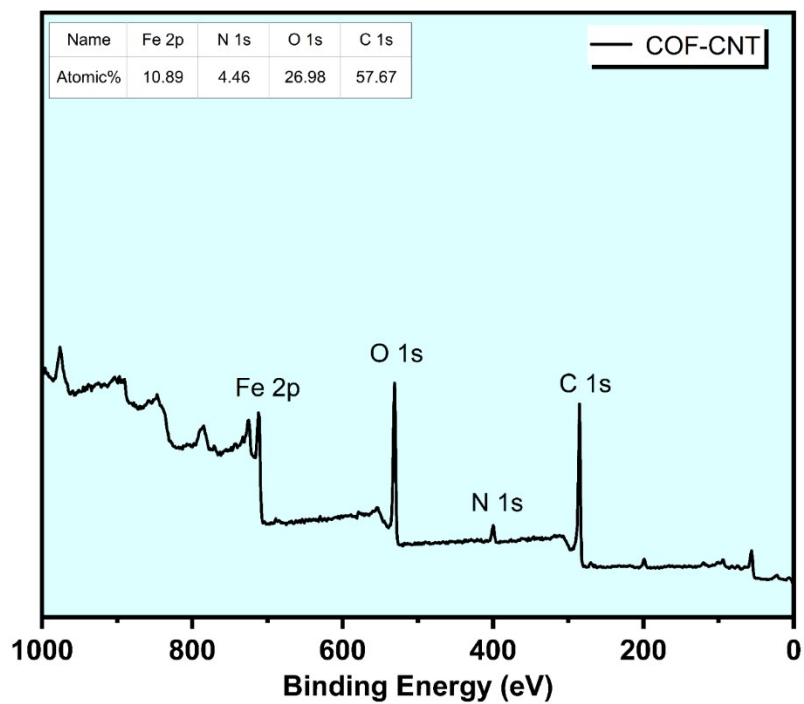
Supplementary Fig. 2. SEM image of COF-CNT.



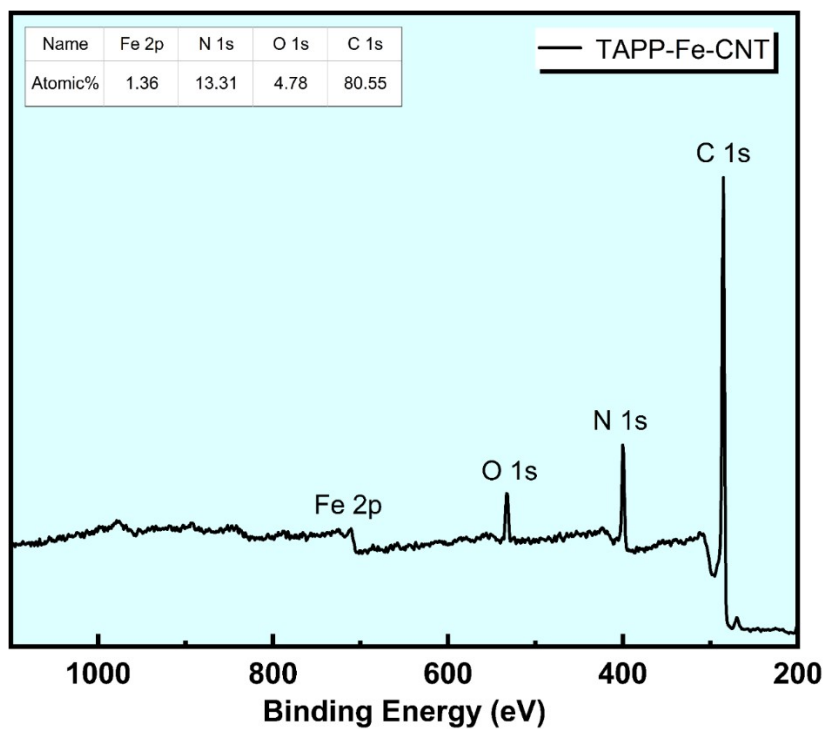
Supplementary Fig. 3. Energy-dispersive X-ray analysis (EDAX) spectrum and corresponding element contents of COF-CNT.



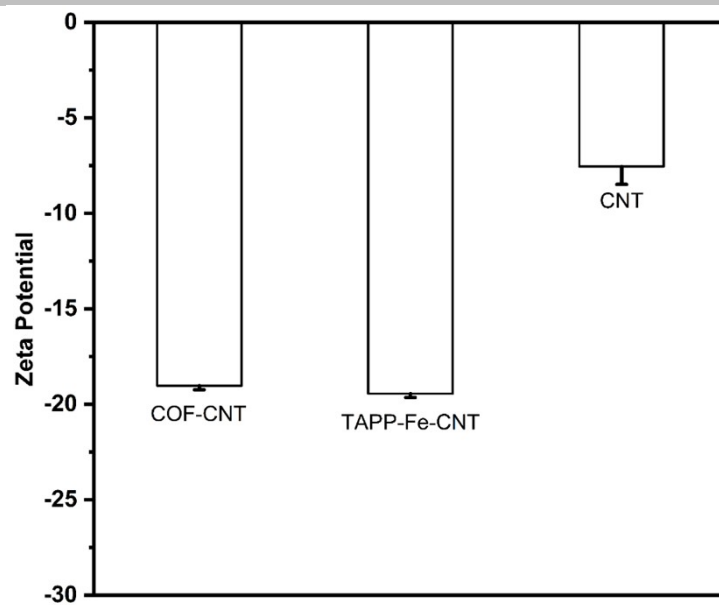
Supplementary Fig. 4. High-resolution C 1s XPS spectrum of COF-CNT.



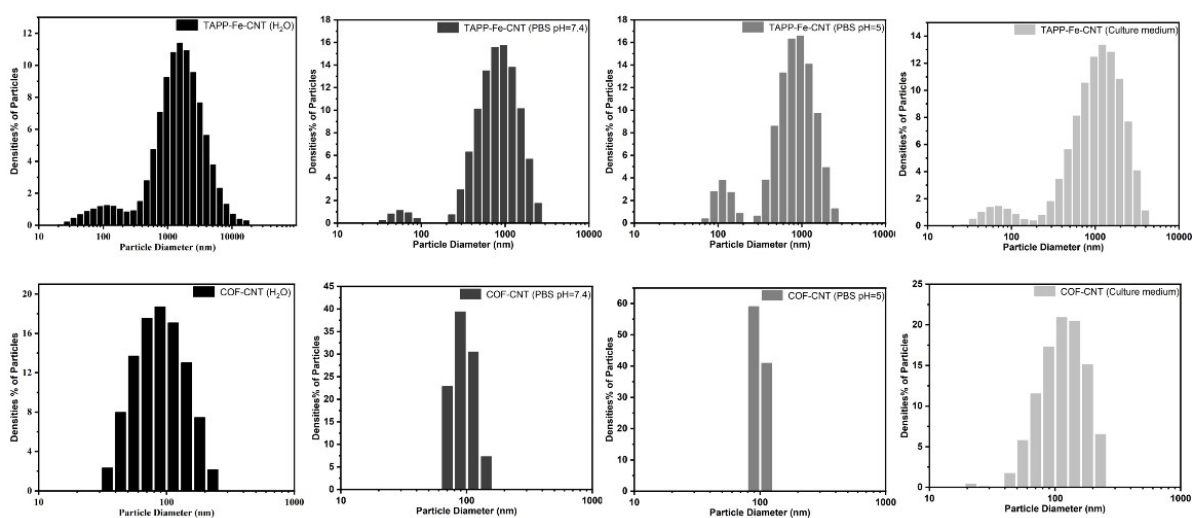
Supplementary Fig. 5. XPS survey spectrum and the calculated element content (inset) of COF-CNT.



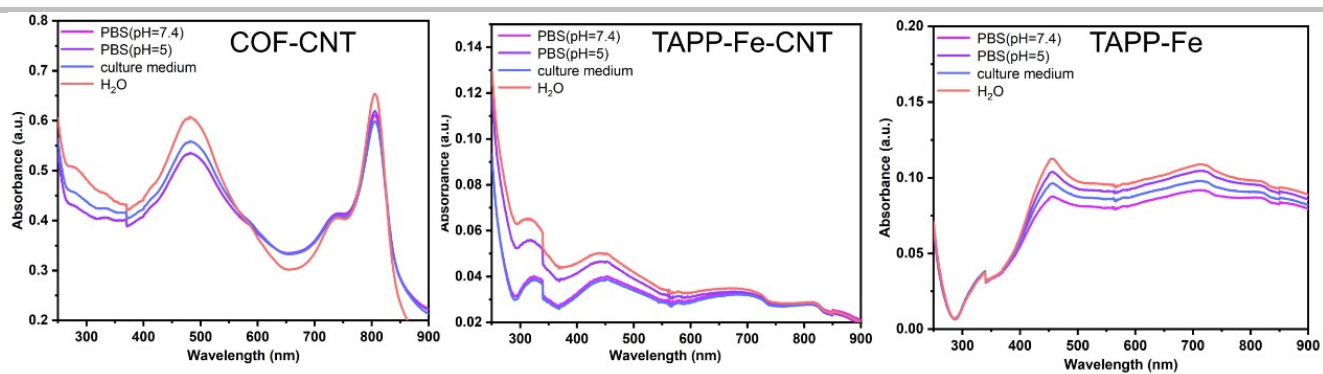
Supplementary Fig. 6. XPS survey spectrum and the calculated element content (inset) of TAPP-Fe-CNT.



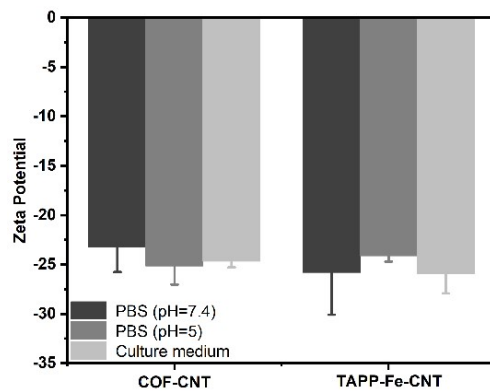
Supplementary Fig. 7. Zeta potential of COF-CNT, TAPP-Fe-CNT and CNT in H₂O.



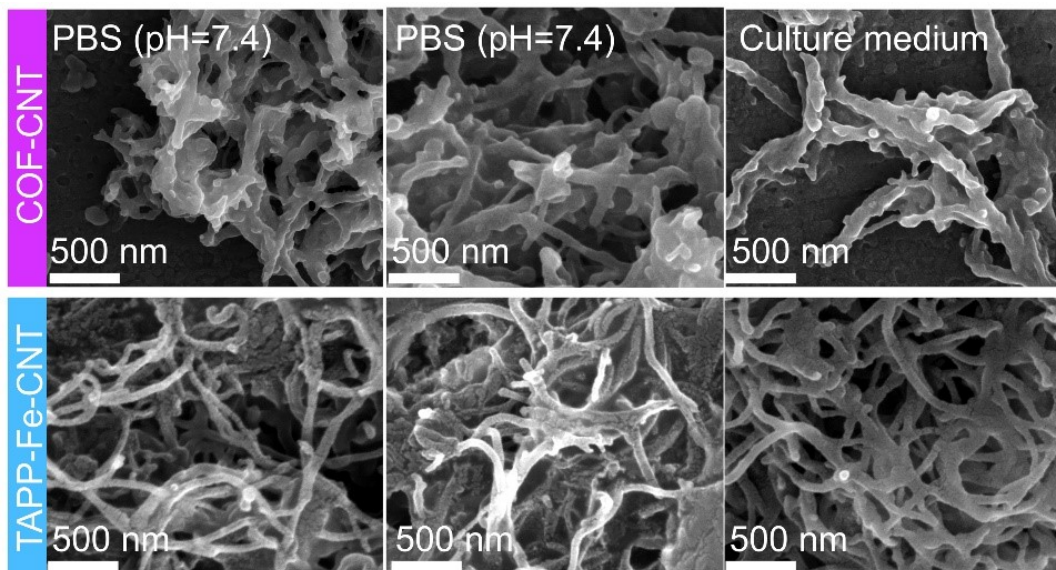
Supplementary Fig. 8. Hydrodynamic size of COF-CNT and TAP-Fe-CNT in H₂O pH 7.4 PBS, pH 5 PBS, and complete cell culture medium supplied with 10% FBS for 24 h and washed with water for 3 times.



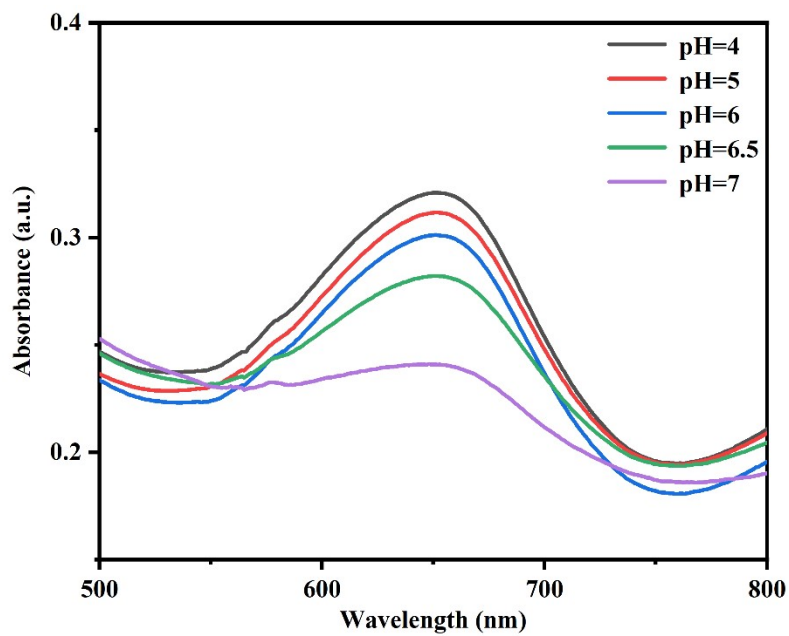
Supplementary Fig. 9. UV-vis absorption spectra of COF-CNT, TAP-Fe-CNT and TAPP-Fe after immersed in H₂O pH 7.4 PBS, pH 5 PBS, and complete cell culture medium supplied with 10% FBS for 24 h and washed with water for 3 times.



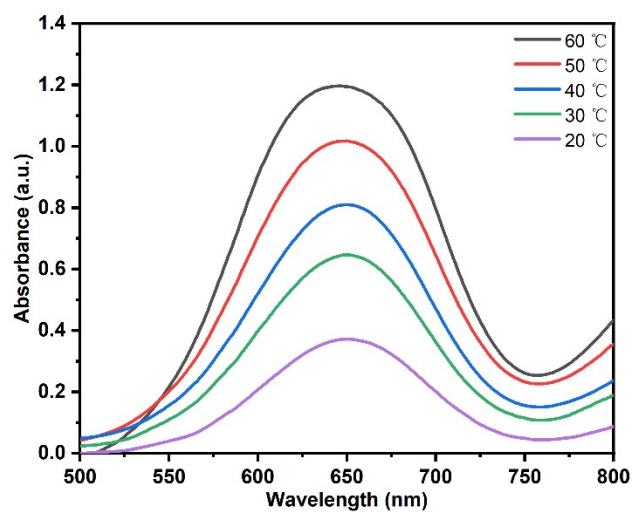
Supplementary Fig. 10. Zeta potential of COF-CNT and TAP-Fe-CNT in pH 7.4 PBS, pH 5 PBS, and complete cell culture medium supplied with 10% FBS for 24 h and washed with water for 3 times.



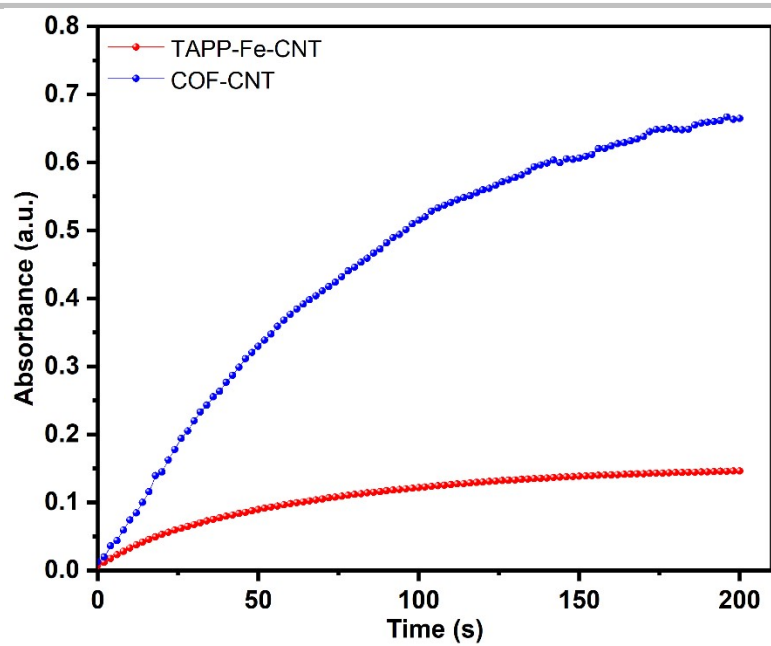
Supplementary Fig. 11. SEM images of COF-CNT and TAP-Fe-CNT in pH 7.4 PBS, pH 5 PBS, and complete cell culture medium supplied with 10% FBS for 24 h and washed with water for 3 times.



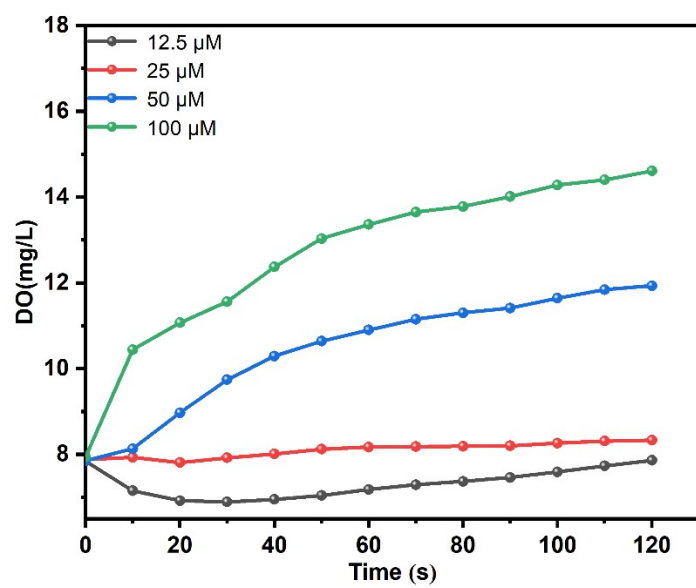
Supplementary Fig. 12. POD-like activities of COF-CNT ($60 \mu\text{g mL}^{-1}$) with $100 \mu\text{M H}_2\text{O}_2$ at different pH (4, 5, 6, 6.5, and 7).



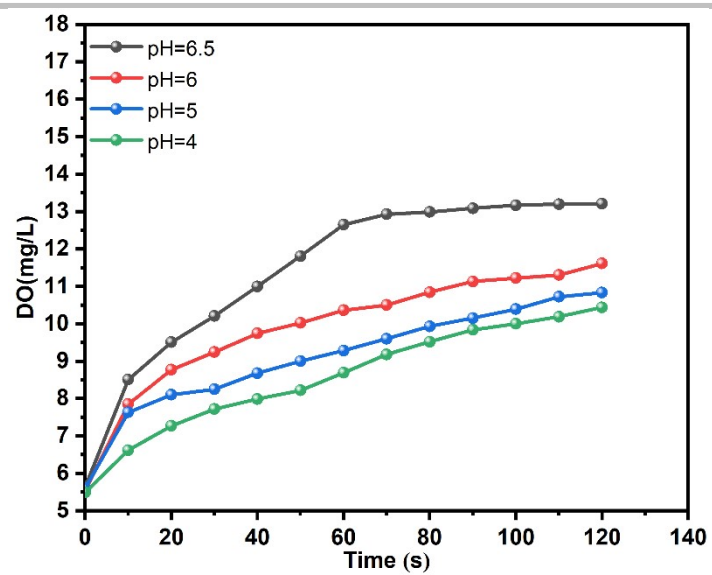
Supplementary Fig. 13. POD-like activities of COF-CNT ($60 \mu\text{g mL}^{-1}$) with $100 \mu\text{M H}_2\text{O}_2$ at different temperature (20, 30, 40, 50 and 60 °C).



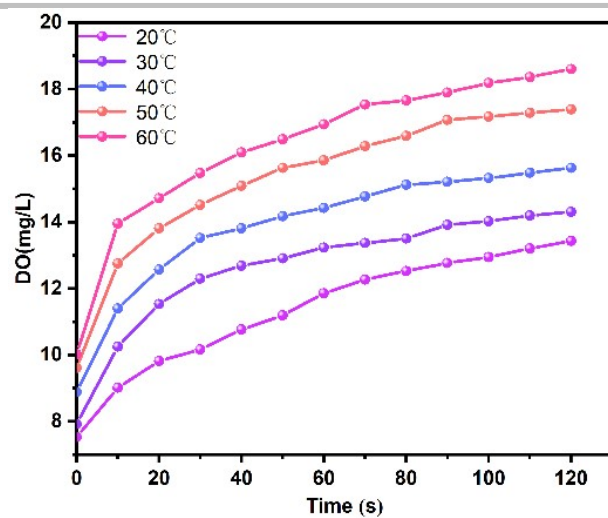
Supplementary Fig. 14. Time-dependent absorbance of oxTMB upon the addition of COF-CNT ($60 \mu\text{g mL}^{-1}$) and TAPP-Fe-CNT ($60 \mu\text{g mL}^{-1}$).



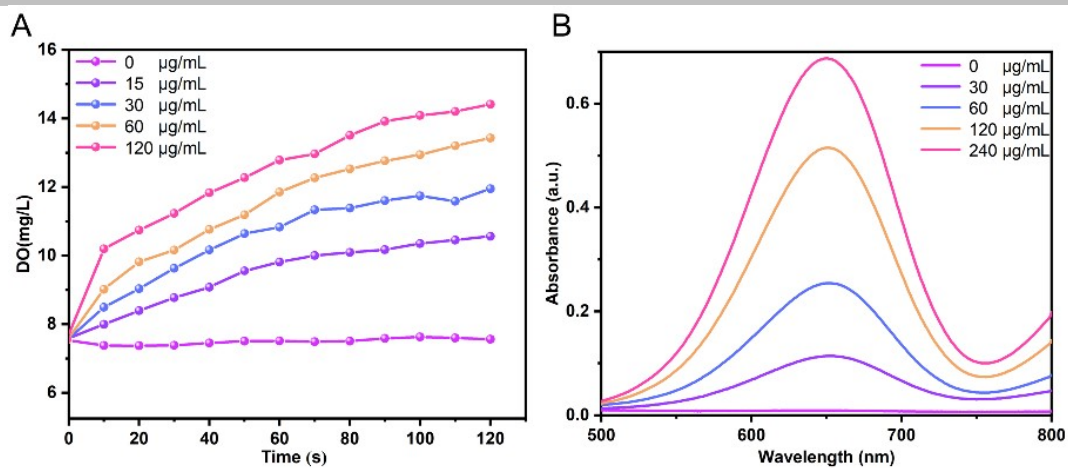
Supplementary Fig. 15. CAT-like activities of COF-CNT ($60 \mu\text{g mL}^{-1}$, $\text{pH}=6.5$) with H_2O_2 of different concentrations (12.5, 25, 50, and 100 μM).



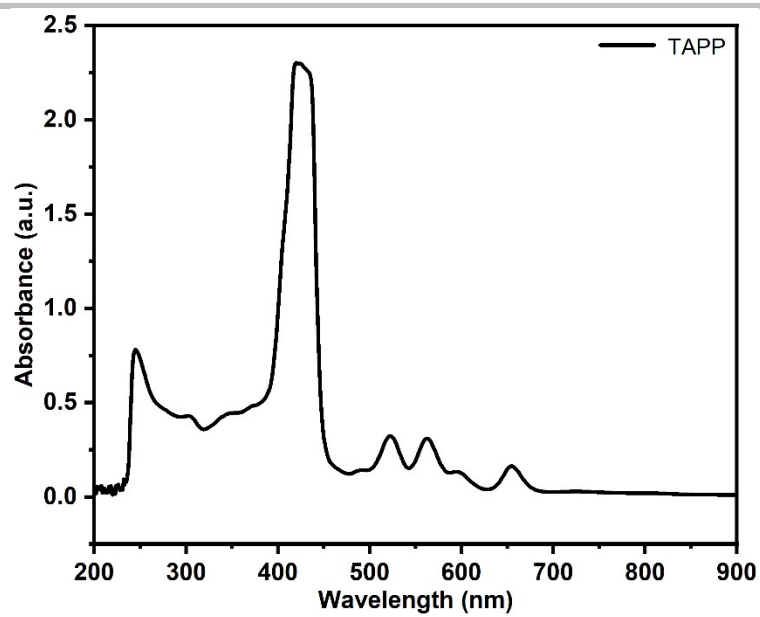
Supplementary Fig. 16. CAT-like activities of COF-CNT ($60 \mu\text{g mL}^{-1}$) with H_2O_2 ($100 \mu\text{M}$) and different pH (4, 5, 6, and 6.5).



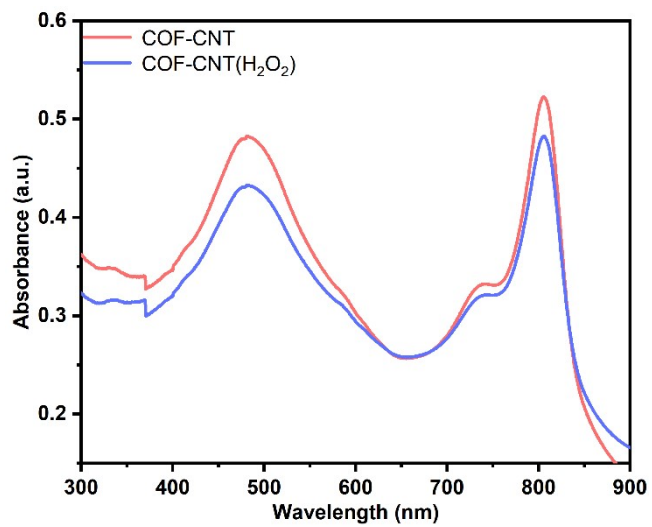
Supplementary Fig. 17. CAT-like activity of COF-CNT ($60 \mu\text{g mL}^{-1}$, $\text{pH}=6.5$) at different temperatures (20, 30, 40, 50 and 60 °C).



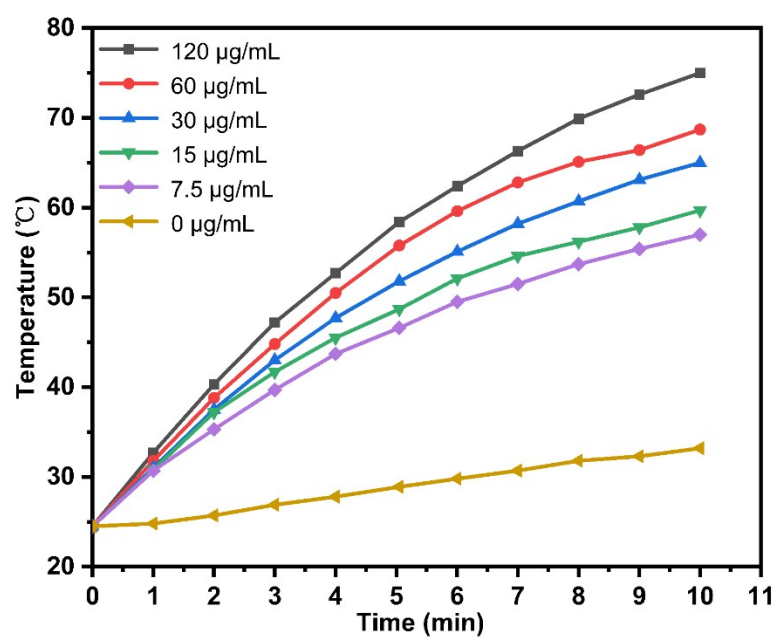
Supplementary Fig. 18. (A) CAT-like activity of COF-CNT (pH=6.5) at different concentrations (0, 15, 30, 60 and 120 $\mu\text{g/mL}$). (B) POD-like activity of COF-CNT (pH=6.5) at different concentrations (0, 30, 60, 120 and 240 $\mu\text{g/mL}$).



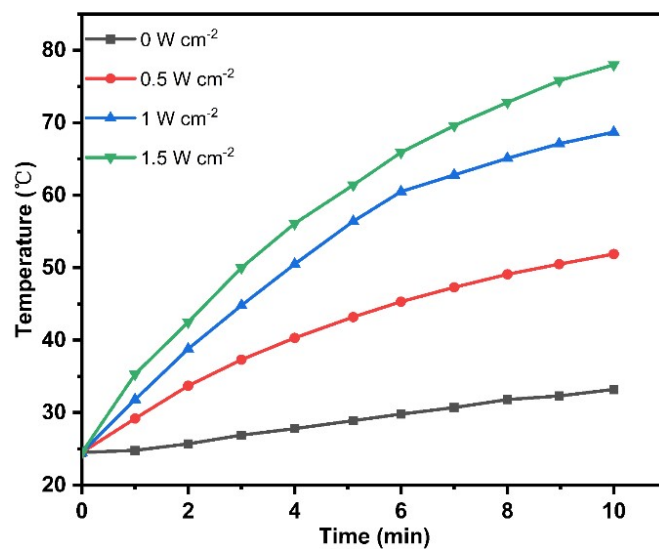
Supplementary Fig. 19. UV-vis absorption spectrum of TAPP.



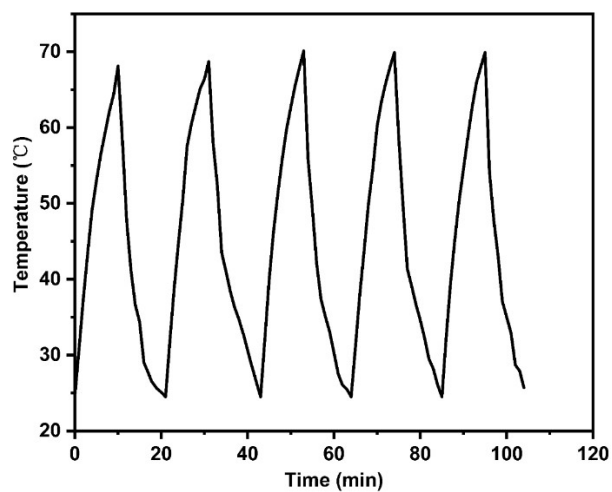
Supplementary Fig. 20. UV-vis absorption spectra of COF-CNT before and after the addition of H₂O₂ (100 μM).



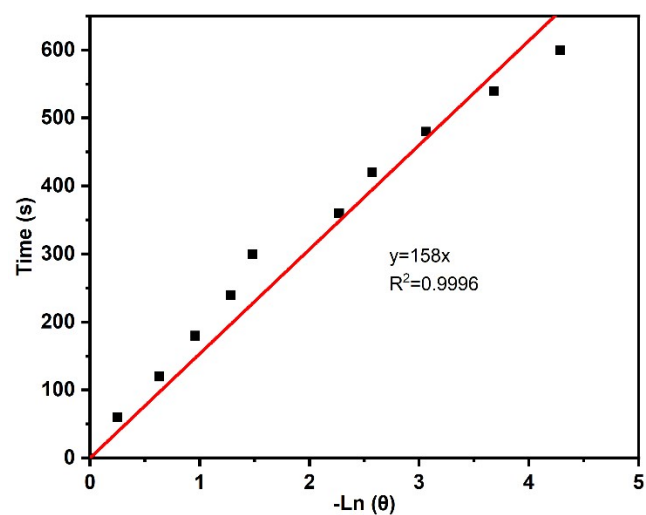
Supplementary Fig. 21. Temperature change of COF-CNT for different concentrations (0, 7.5, 15, 30, 60 and 120 µg/mL) under 808 nm laser irradiation (1 W cm^{-2}).



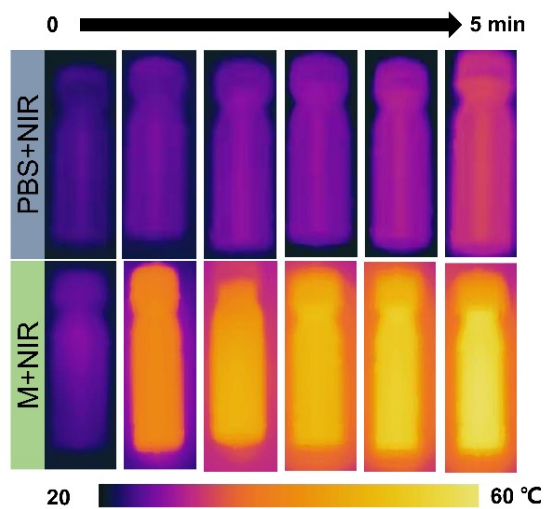
Supplementary Fig. 22. Temperature change of COF-CNT ($60 \mu\text{g mL}^{-1}$, 1 mL) under 808 nm laser irradiation with different power densities (0, 0.5, 1, and 1.5 W cm^{-2}).



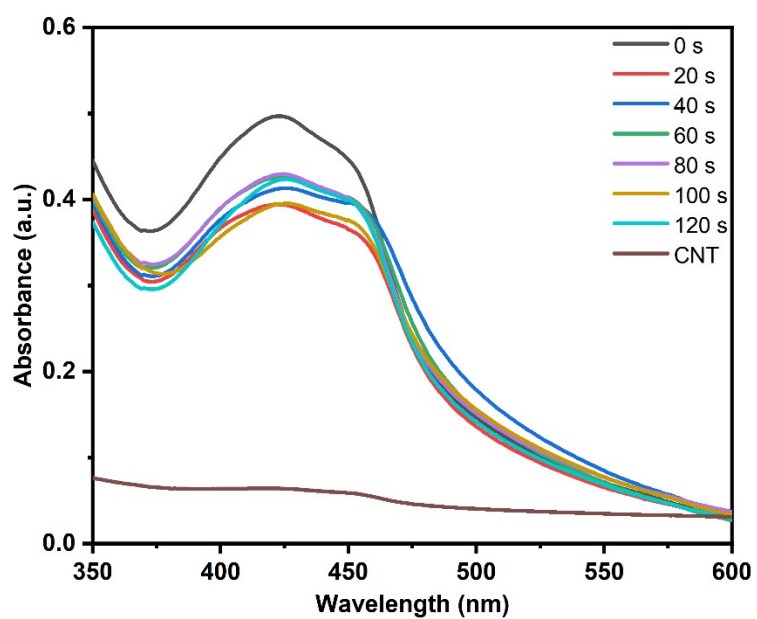
Supplementary Fig. 23. Photothermal stability test of COF-CNT ($60 \mu\text{g mL}^{-1}$, 1 mL) under 808 nm laser irradiation (1 W cm^{-2}).



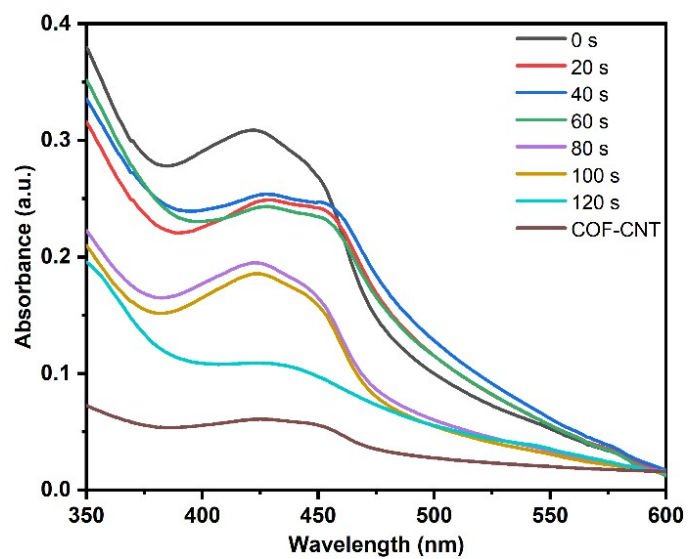
Supplementary Fig. 24. Photothermal conversion efficiency curve of COF-CNT.



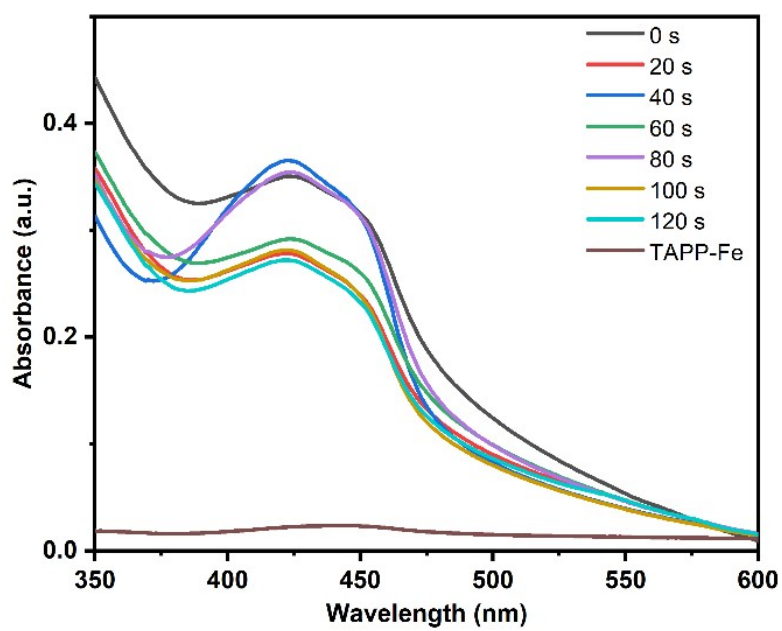
Supplementary Fig. 25. Infrared thermal images of PBS and COF-CNT with concentration of $60 \mu\text{g mL}^{-1}$ under 808 nm laser irradiation (1.0 W cm^{-2}) for 5 min.



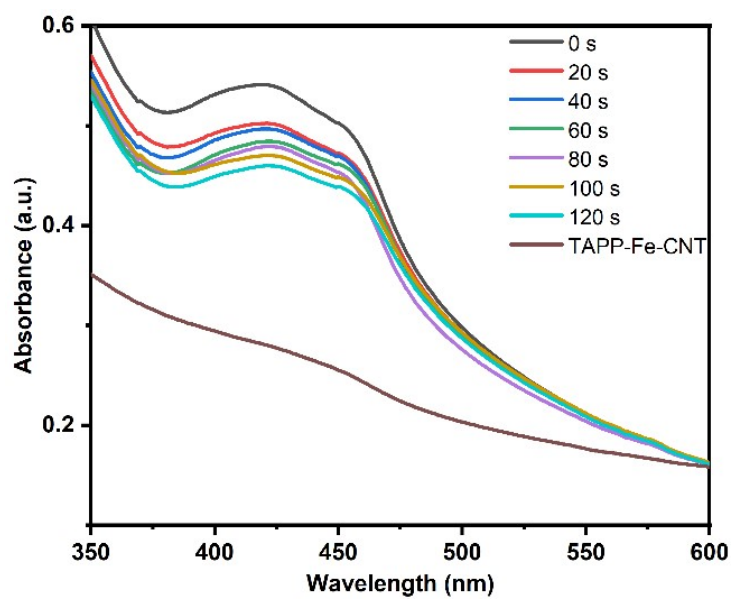
Supplementary Fig. 26. The degradation of DPBF by CNT aqueous solution ($60 \mu\text{g mL}^{-1}$, $\text{pH}=6.5$) at different time intervals.



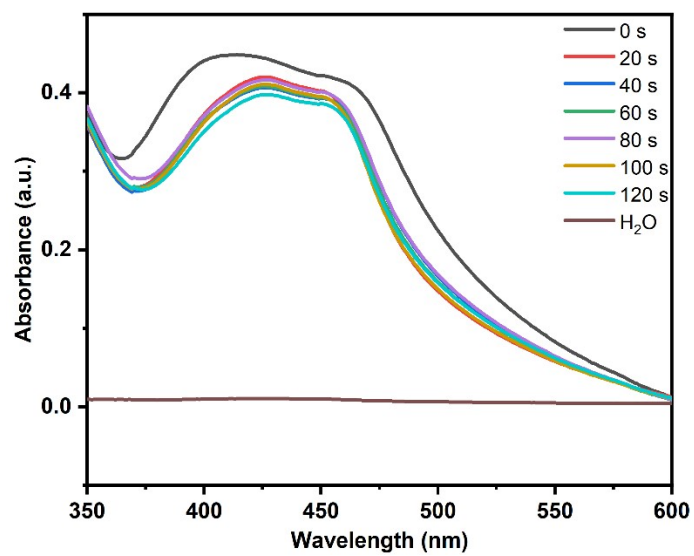
Supplementary Fig. 27. The degradation of DPBF by COF-CNT aqueous solution ($60 \mu\text{g mL}^{-1}$, $\text{pH}=6.5$) at different time intervals.



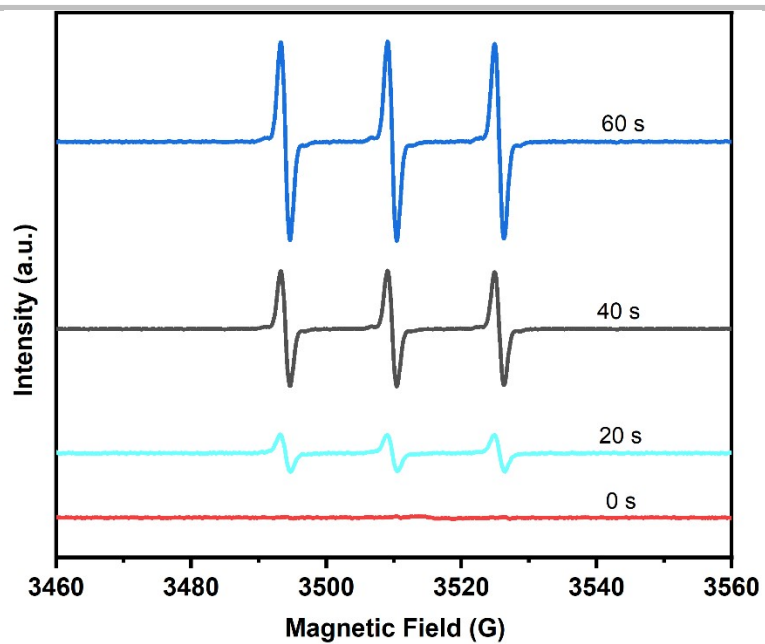
Supplementary Fig. 28. The degradation of DPBF by TAPP-Fe aqueous solution ($60 \mu\text{g mL}^{-1}$, $\text{pH}=6.5$) at different time intervals.



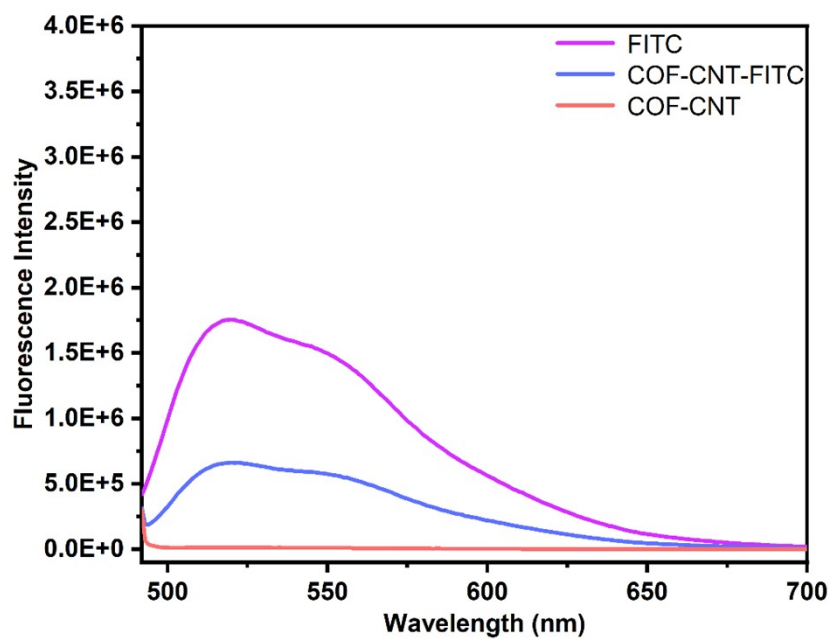
Supplementary Fig. 29. The degradation of DPBF by TAPP-Fe-CNT aqueous solution ($60 \mu\text{g mL}^{-1}$, $\text{pH}=6.5$) at different time intervals.



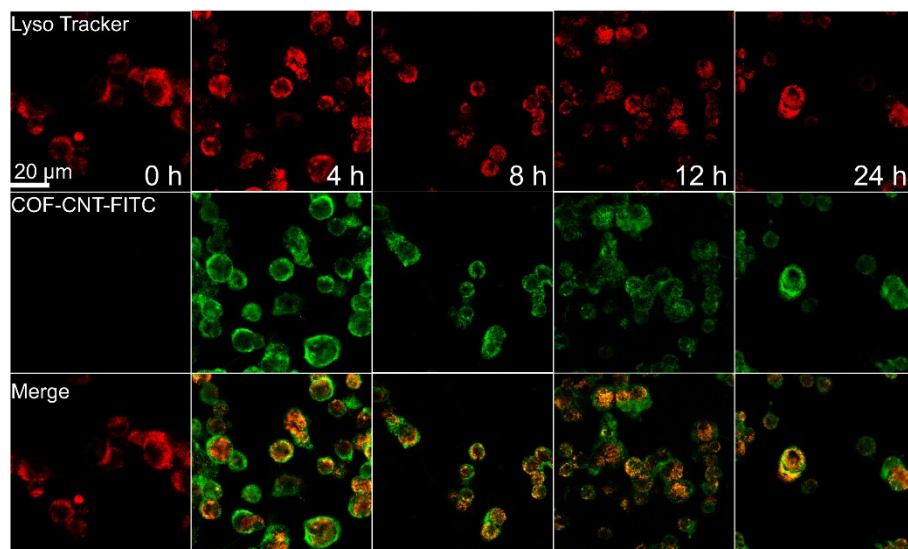
Supplementary Fig.30. The degradation of DPBF by H₂O aqueous solution (pH=6.5) at different time intervals.



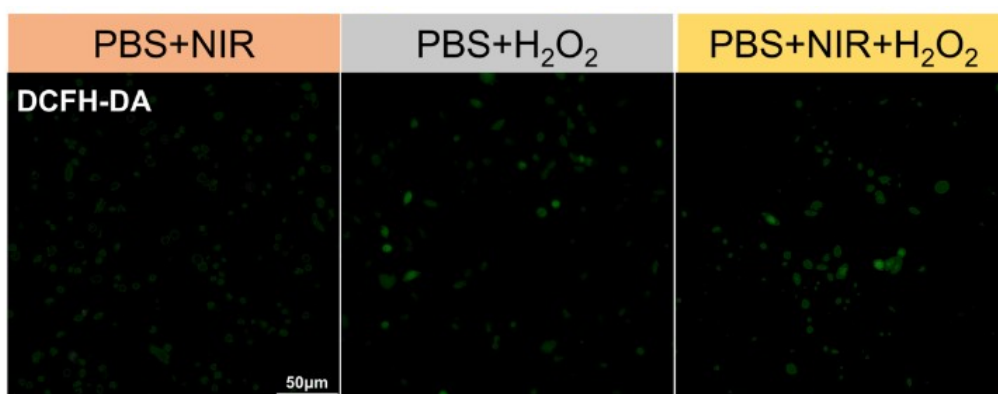
Supplementary Fig. 31. ESR spectra of PBS solution (pH=6.5) containing COF-CNT under different time of NIR light irradiation using 2,2,4,4-tetramethyl-1-piperidinyloxy (TEMPO) as the trapping agent.



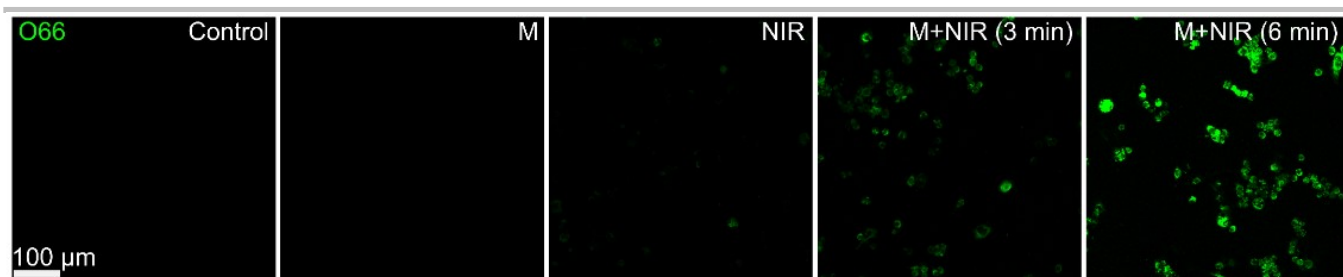
Supplementary Fig. 32. Fluorescence spectra of FITC, COF-CNT, and COF-CNT-FITC. For observing the cell uptake, fluorescent FITC was tethered onto COF-CNT through Schiff-base reaction.



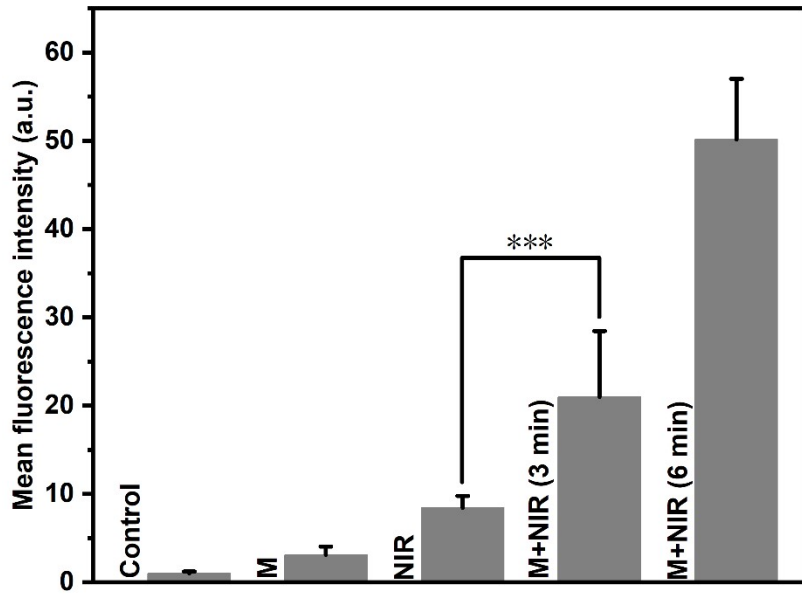
Supplementary Fig. 33. Fluorescence colocalization images of COF-CNT with Lyso Tracker RED in 4T1 cells. After different-time-intervals addition of $60 \mu\text{g mL}^{-1}$ COF-CNT into the 4T1 cells (4, 8, 12, and 24 h), the cells were co-stained with Lyso-Tracker RED and observed. The results showed that most of COF-CNT located on the surface of cell membrane at 4 h. From 8 h to 24 h, a partial of COF-CNT were co-localized with endosomes/lysosomes (yellow color showing merge of red and green), and the others were located in cytoplasm (green color).



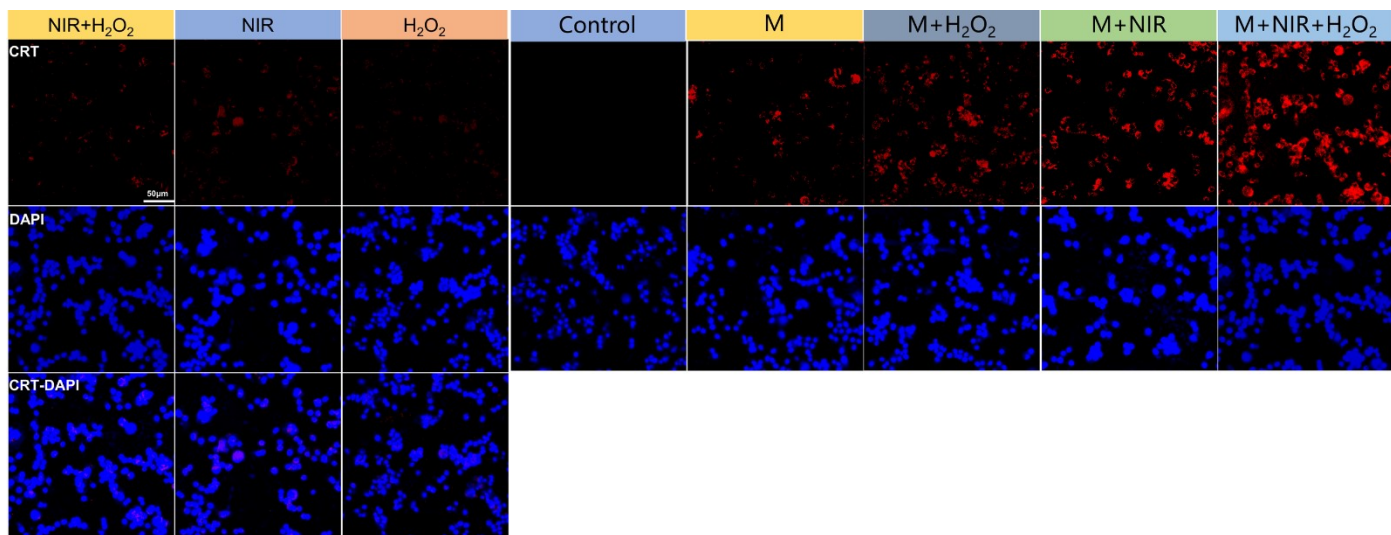
Supplementary Fig. 34. CLSM images of 4T1 cells staining by DCFH-DA.



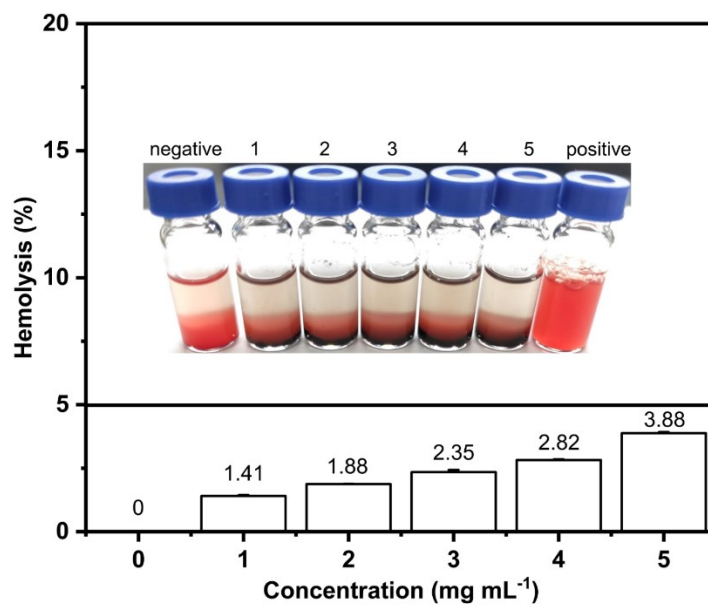
Supplementary Fig. 35. Confocal laser scanning microscope images of 4T1 cells with different treatments and stained with ¹O₂ detection probe O66 (λ_{ex} : 488 nm; λ_{em} : 520–530 nm).



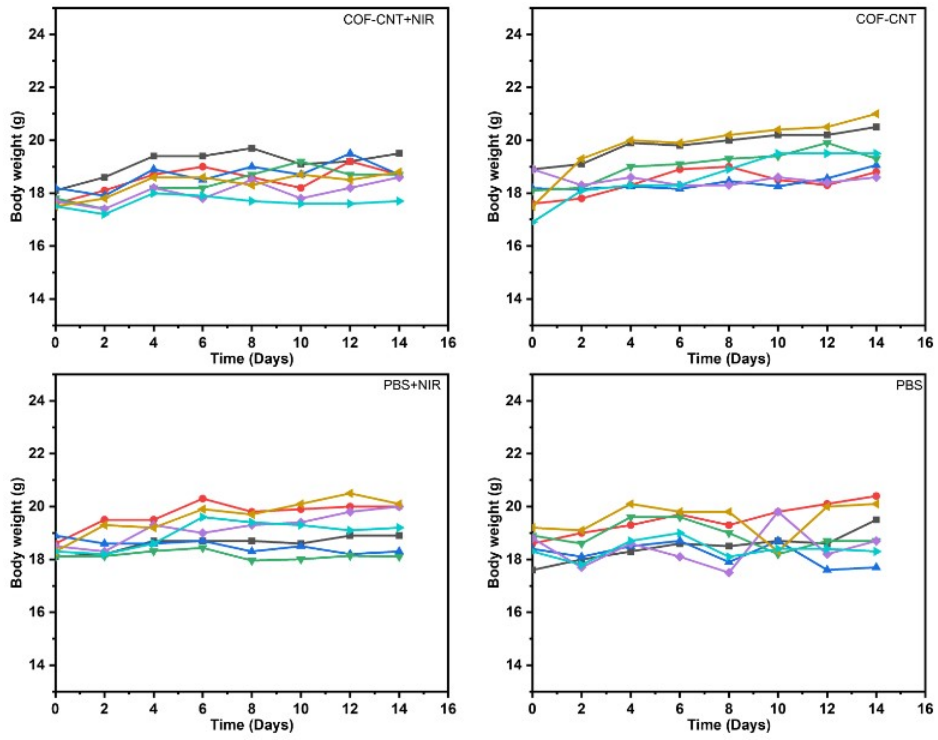
Supplementary Fig. 36. Relative intensity of corresponding green fluorescence in Supplementary Fig. 35 under different treating conditions.



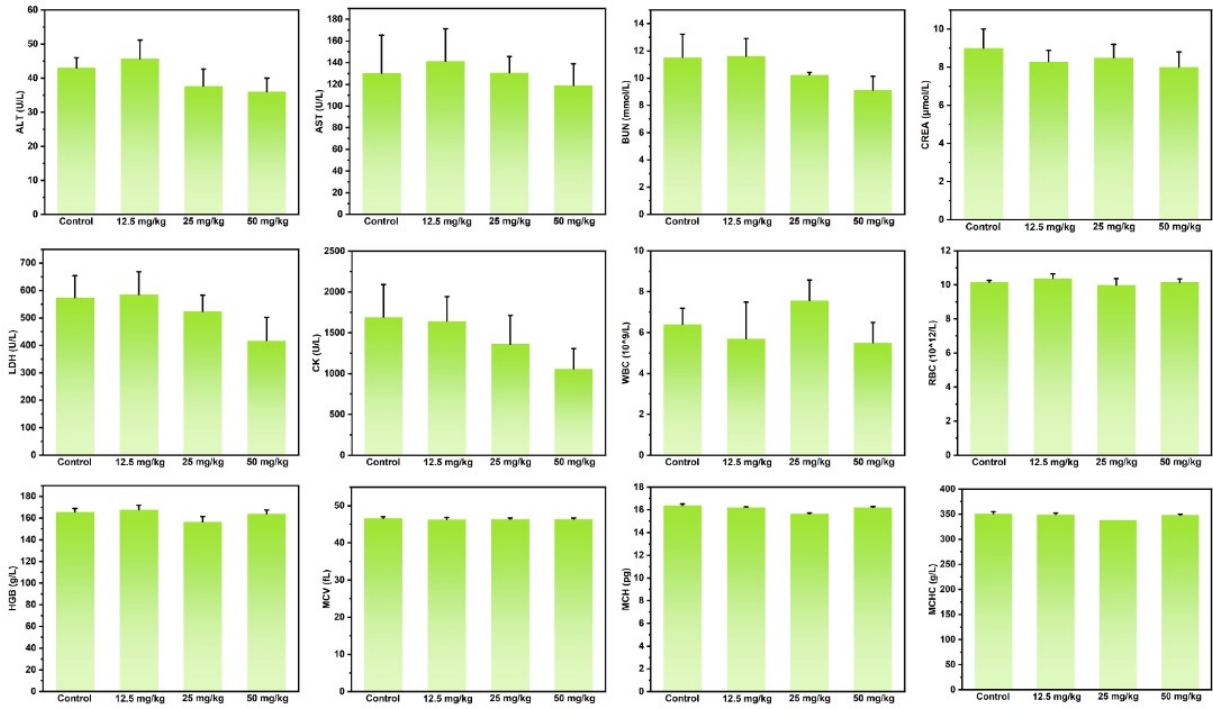
Supplementary Fig. 37. Confocal images of 4T1 cells staining by CRT antibody and DAPI.



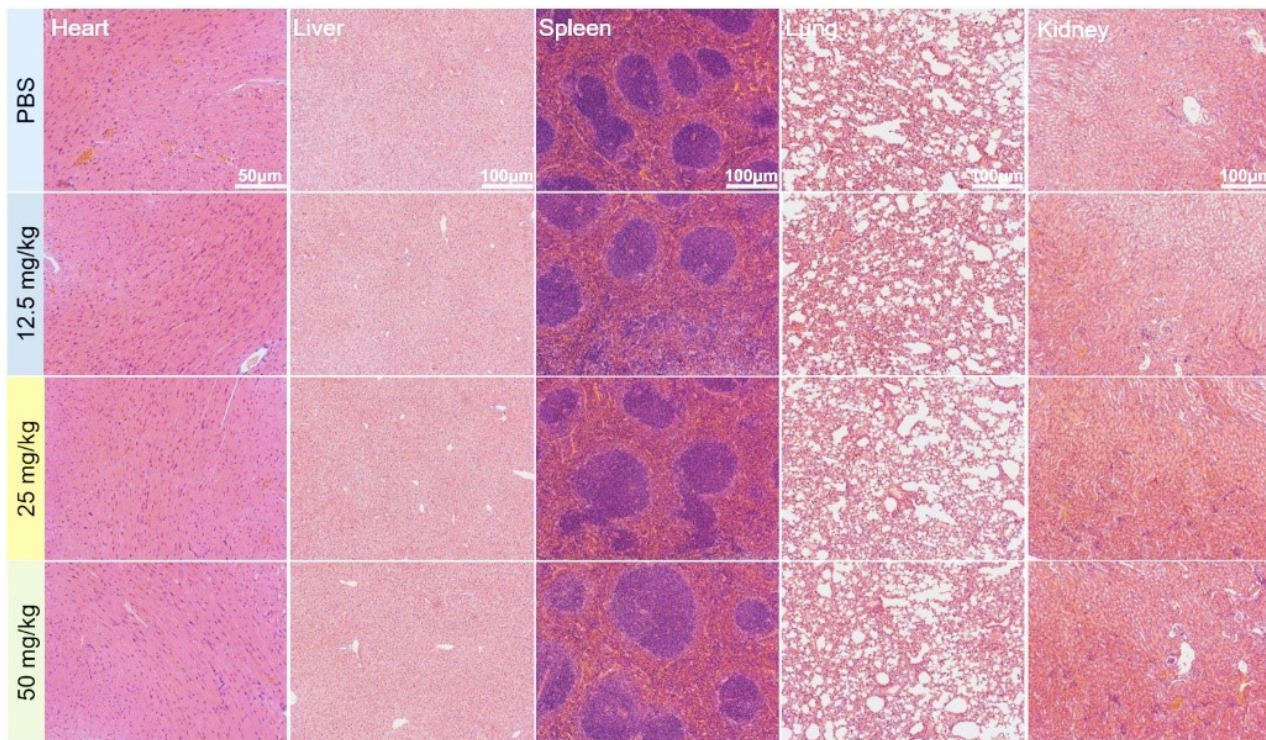
Supplementary Fig. 38. The percentage of hemolysis with different concentrations of COF-CNT. The inset shows the hemolysis with different concentrations of COF-CNT, negative control and positive control.



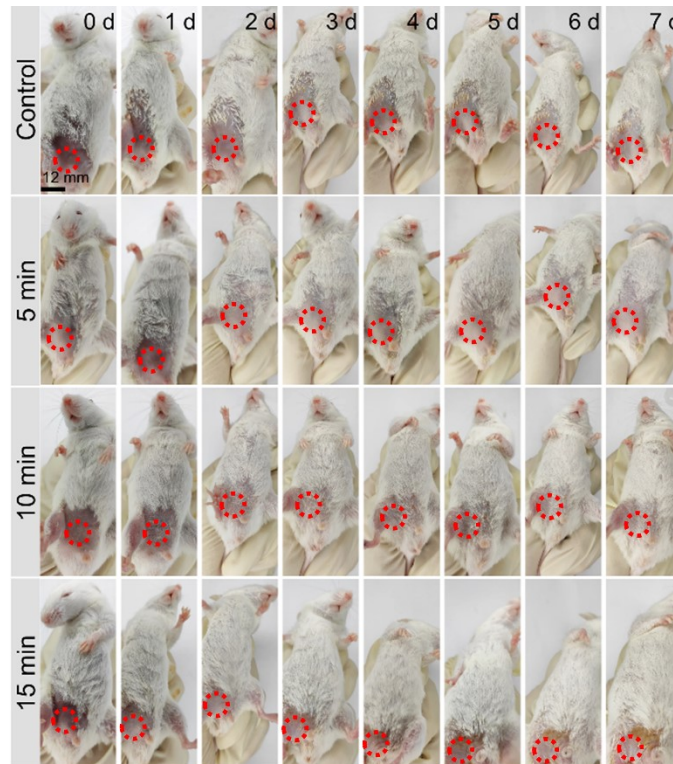
Supplementary Fig. 39. Body weight of mice in different groups during 14 days of treatments.



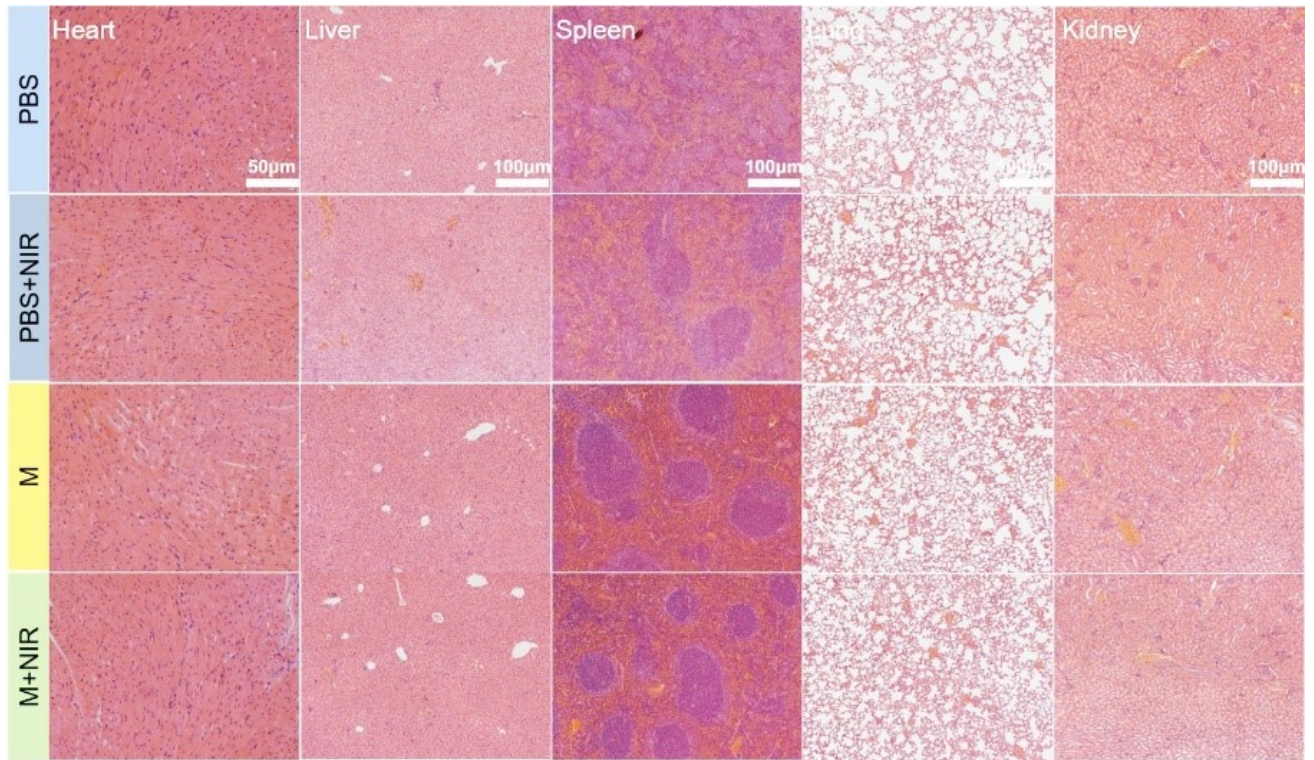
Supplementary Fig. 40. The blood routine and blood biochemistry examination of mice after intravenous injection with different doses of COF-CNT and PBS, respectively.



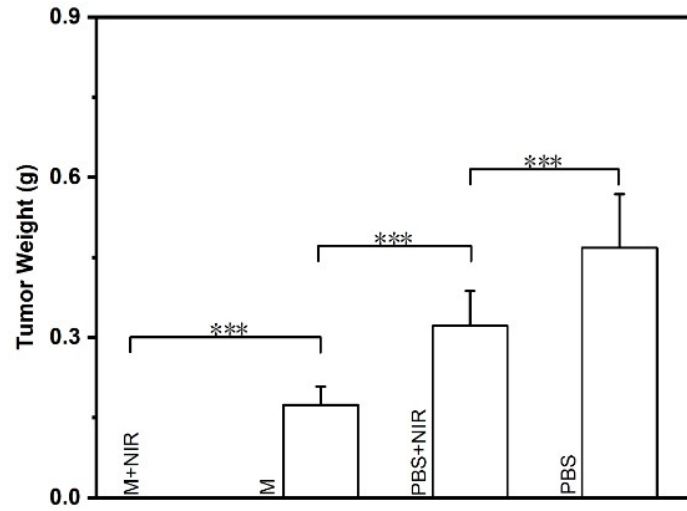
Supplementary Fig. 41. In vivo systematic toxicity after intravenous injection of COF-CNT with different concentrations. Representative H&E stained histological images of heart, liver, spleen, lung and kidney.



Supplementary Fig. 42. Photographs of healthy mice after 808 nm laser irradiation (1 W cm^2) for different times. The results showed that the skin of mice did not change significantly after irradiation for 5 min and 10 min. In comparison, when the mouse was irradiated for 15 min, a slight yellow scab appeared on the mouse skin on the 3rd day, which was disappeared with the prolonging of time. The red circles in each photo mark the location of laser irradiation.



Supplementary Fig. 43. Representative H&E stained histological images of heart, liver, spleen, lung and kidney from 4T1 tumor-bearing mice after different treatments.



Supplementary Fig. 44. Mean tumor weights after excision at day 14 (n =7). *P< 0.01, **P< 0.005, and ***P<0.001.

Supplementary Tables

Supplementary Table 1. Average hydrodynamic diameter, polydispersity index, and Zeta potential of COF-CNT and TAPP-Fe-CNT in pH 7.4 PBS, pH 5 PBS, and complete cell culture medium supplied with 10% FBS for 24 h and washed with water for 3 times via dynamic light scattering.

Sample	Average Hydrodynamic Diameter (nm)	Polydispersity Index	Average Zeta Potential (mV)
TAPP-Fe-CNT (H ₂ O)	926	0.527	-19.442±2.125
TAPP-Fe-CNT (PBS pH=7.4)	892	0.395	-25.8075±4.26
TAPP-Fe-CNT (PBS pH=5)	914	0.392	-24.12±1.41
TAPP-Fe-CNT (Culture medium)	986	0.532	-25.93667±4.163
COF-CNT (H ₂ O)	87	0.013	-19.024±1.012
COF-CNT (PBS pH=7.4)	93	0.008	-23.2275±2.229
COF-CNT (PBS pH=5)	98	0	-25.15667±2.871
COF-CNT (Culture medium)	126	0.022	-24.67667±3.98

Supplementary Table 2. The catalytic activities of COF-CNT and TAPP-Fe-CNT.

Catalysts	Substrates	Km (mM)	Vmax (mM s ⁻¹)	V (mM s ⁻¹)
COF-CNT	TMB	1.471	0.0082	0.0034
TAPP-Fe-CNT	TMB	0.217	0.0029	0.0024

Supplementary Table 3. Change of free energy in each step for the POD-like catalytic process.

$\Delta G(\Delta G = \Delta E + \Delta ZPE - T\Delta S)$ (eV)	COF-CNT	TAPP-Fe-CNT
I: *+H ₂ O ₂ =*OH+*OH	-1.27	-1.39
II: *OH+*OH=*OH+*OH	0.39	0.47
III: *OH+H ⁺ +e ⁻ =*+H ₂ O	-0.65	-0.61

In this formula, $\Delta G = \Delta E + \Delta ZPE - T\Delta S$, ΔE is the chemisorption energy of the molecules before and after the reaction. ΔZPE is the difference in zero point energy between the adsorbed and the gas phase. $\Delta S = -1/2 S_0$, where S_0 is the entropy of the products in the gas phase at standard conditions.

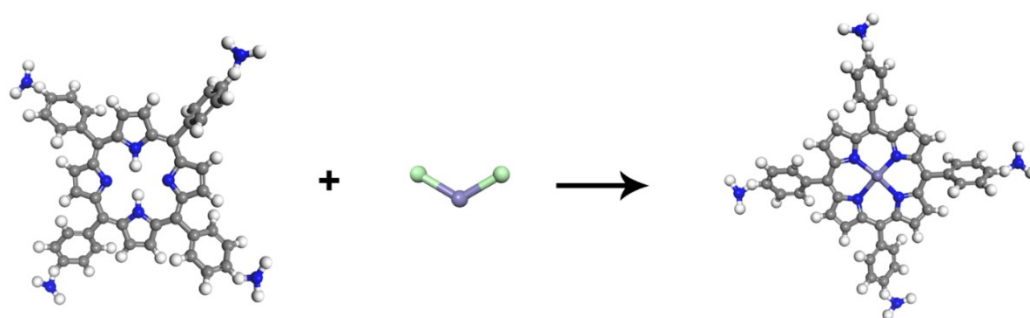
Supplementary Table 4. Change of free energy in each step for the CAT-like catalytic process.

$\Delta G(\Delta G = \Delta E + \Delta EZPE - T\Delta S)$ (eV)	COF-CNT	TAPP-Fe-CNT
I: *+H ₂ O ₂ +OH=*OOH+H ₂ O+e ⁻	-0.42	-0.43
II: *OOH+OH=*OO+H ₂ O+e ⁻	0.58	0.57
III: *OO=*+O ₂	0.84	0.86

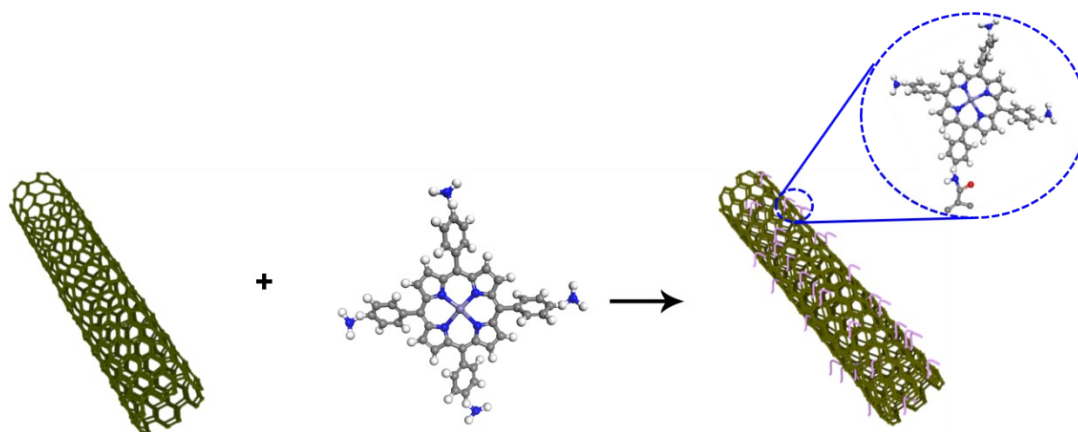
Supplementary Table 5. Mass ratio of samples measured by ICP-AES.

Samples	Fe content (%)
TAPP-Fe-CNT	1.84
COF-CNT	2.5

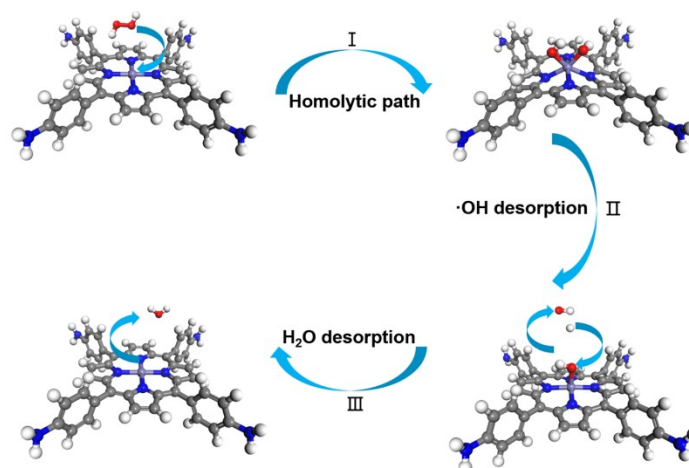
Supplementary Schematics



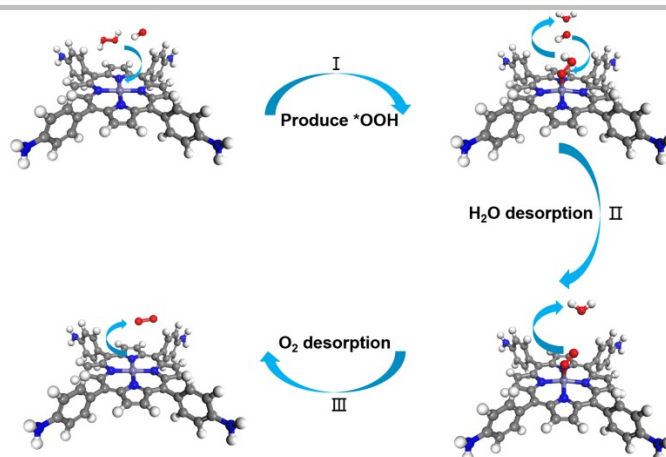
Supplementary Scheme 1. Schematic representation of the reaction of TAPP with FeCl₂ to prepare TAPP-Fe.



Supplementary Scheme 2. Schematic representation of reaction to tether TAPP-Fe onto carboxyl CNTs.
SI-20 Schematic illustration of the POD-/CAT-like catalytic reaction mechanism

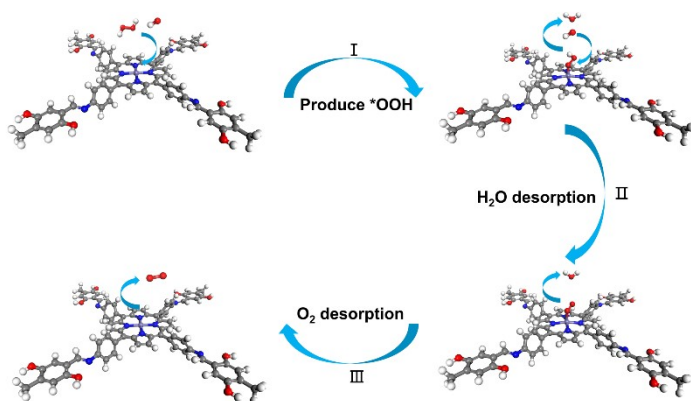


Supplementary Scheme 3. Schematic illustration of the POD-like catalytic reaction mechanism for TAPP-Fe-CNT.

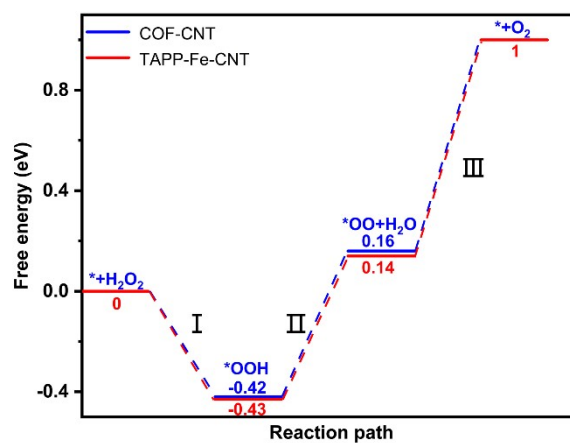


Supplementary Scheme 4. Schematic illustration of the CAT-like catalytic reaction mechanism for TAPP-Fe-CNT.

A



B



Supplementary Scheme 5. (A) Schematic illustration of the proposed reaction mechanism for the production process of O₂ for TAPP-Fe-CNT. (B) Free energy diagram for the production process of O₂ for TAPP-Fe-CNT.

Supplementary References

- 1 Kresse, G. & Joubert, D. From ultrasoft pseudopotentials to the projector augmented-wave method. *Physical Review B* 1999, **59**, 1758-1775.
- 2 Perdew, J. P., Burke, K. & Ernzerhof, M. Generalized Gradient Approximation Made Simple. *Phys Rev Lett* 1996, **77**, 3865-3868.
- 3 Nørskov, J. K., Bligaard, T., Logadottir, A. *et al.* Trends in the Exchange Current for Hydrogen Evolution. *Journal of The Electrochemical Society* 2005, **152**, J23.